EFFECTS OF PLASMA-ACTUATOR-GENERATED VORTICES ON A TURBULENT BOUNDARY LAYER

Chi Wai Wong

Shenzhen Graduate School
Harbin Institute of Technology
Shenzhen 518055, P.R. China
cwwong@hit.edu.cn

Xiaoqi Cheng

Shenzhen Graduate School
Harbin Institute of Technology
Shenzhen 518055, P.R. China
chengxiaoqi1990@163.com

Qian Peng

Shenzhen Graduate School
Harbin Institute of Technology
Shenzhen 518055, P.R. China
1830102933@qq.com

Yu Zhou

Shenzhen Graduate School
Harbin Institute of Technology
Shenzhen 518055, P.R. China
yuzhou@hit.edu.cn

ABSTRACT

This work presents the investigation on the control of a fully developed turbulent boundary layer (TBL) over a flat plate based on plasma-induced streamwise vortices aiming for drag reduction. Three plasma actuator configurations are explored for generating streamwise vortices of different sizes and strength. Dependence of various parameters, including the size of actuator-generated vortex, the actautor yaw angle β and the actuator length L, on the drag change have been examined. Hotwire and the surface balance techniques are deployed to capture the drag change. Given the same applied voltage, it is found that the large streamwise vortices generated by the very long actuator (L = 300 mm) and their interactions with the boundary layer leads to the maximum drag reduction of 25%.

INTRODUCTION

Drag reduction in turbulent boundary layers (TBL) has received widespread attention in literature and its potential benefits in various engineering applications cannot be overlooked.

The control of turbulent boundary-layer aiming for high skin-friction drag reduction always depends on an effective flow control device. Dielectric barrier discharge (DBD) plasma actuator is a relatively new active control device but is experiencing a rapid development due to its simple structure, rapid response and no moving parts. The simplest arrangement of DBD plasma actuator typically consists of a pair of electrodes separated by dielectric material, and an alternating voltage is applied across the electrodes, resulting in the generation of plasma in the vicinity of the electrodes. Plasma actuator is rather extensively used for the laminar and turbulent flow separation control on streamlined and bluff bodies. See Moreau (2007) and Corke et al. (2010) for recent reviews on plasma actuators for aerodynamic applications. Choi et al. (2011) studied two configurations of DBD plasma actuators for the control of a TBL over a flat plate. Their DBD plasma actuators were aligned in the streamwise direction to produce forcing along the spanwise direction. Both spanwise oscillation and spanwise travelling waves could be produced, depending on the direction of the induced flow of each actuator. Their manipulation modified the near-wall flow structures. Based on their previous experimental findings associated with other flow control devices (e.g. Choi et al. 1998; Choi & Clayton 2001), they suggested that the DBD plasma-actuator-generated spanwise oscillation and travelling waves could lead to a drag reduction of 45%, though the drag change was never measured in their investigation. Recently, Whalley & Choi (2014) indicated that the streamwise counter-rotating vortices, resulted from the plasma-generated bidirectional spanwise travelling waves, lifted up the low-speed streaks from the near-wall region and around the peripheries of their cores, therefore manipulating the turbulence events for drag reduction.

To the author's best knowledge, successful drag reduction in a TBL based on DBD plasma actuators is rather scarce. Previously, we investigated experimentally the plasma-generated vortices for the control of a TBL over a flat plate, and managed an average skin-friction drag reduction up to 20% (Wong et al. 2015). The plasma-generated vortices made a pronounced effect on the flow structures all the way up to $y^+ \leqslant 100$. The upwash of plasma-generated counter-rotating vortex pair pumped the low-momentum fluid away from the wall, leading to a region of lower-speed and stabilized fluid near wall. However, many aspects of skin-friction drag reduction based on DBD plasma actuators have yet to be clarified. For instance, how does the size of plasma-generated vortices influence the local and the spanwise distribution of drag reduction behind the actuators? Given the same applied voltage V_a, how does the length of the actuator affect the drag reduction?

EXPERIMENTAL DETAILS

The study is performed in a closed-circuit low-speed wind tunnel that has a test section with $L \times W \times H$ = 5.0 × 0.8 × 1.0 m. With its leading-edge tripped, a smooth Perspex flat plate generates a fully developed turbulent boundary layer under zero streamwise pressure gradient (Fig. 1). The freestream velocity U_∞ at the entrance of the test section is set at 2.4 m/s, whose

longitudinal turbulence intensity is approximately 0.4%. The turbulent boundary-layer thickness δ is 85 mm at 3.2 m downstream from the leading edge of the flat plate, where most measurements are performed. The Reynolds number based on momentum thickness Re_θ is 1100. The wall unit length l = 150 μm without perturbation.

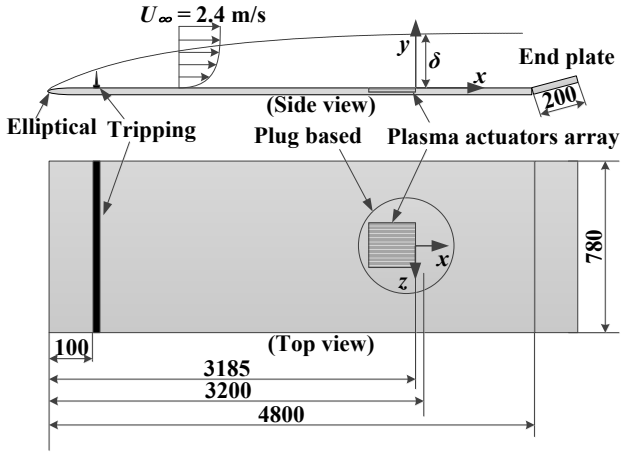

Figure 1. Schematic of the experimental setup.

Three DBD plasma actuator configurations are explored for generating streamwise vortices of different sizes and strength. Configuration A consists of two streamwise-oriented copper electrodes separated by a dielectric panel made of PMMA. The electrode length L of configuration A is defined as the distance between the leading edge and the trailing edge of the upper electrode. Different L (20, 60 and 100 mm) have been investigated to control the vortex size (Fig. 2a). The maximum streamwise vorticity is controlled at an approximately constant value (200 s^{-1}) through tuning V_a. The spacing D between an actuator pair is determined by the size of the vortices generated by the actuator. The selection of D is important because configuration A generates counter-rotating vortex pair, and the vortices do not collide with each other along the entire L. Configuration B is similar to that of A, but the electrodes are yawed at an angle β from the mean flow direction (Fig. 2b). Both A and B are flush-mounted to the wall surface, and the protrusion of the upper electrode from the wall is negligible. Configuration C consists of two copper electrodes separated by a dielectric panel comprised of Kapton and Mylar sheets (Fig. 2c), which gives an overall thickness of about 230 μm (≈ 1.5l). The D is fixed at 60 mm for configuration C. Note that the dielectric material of C differs from that used in A and B to generate substantially weaker counter-rotating vortex pair. Plasma is generated by applying a sinusoidal AC waveform to the upper electrodes with V_a = 3.5 – 15.0 $kV_{p\text{-}p}$ (subscript p-p denotes peak-to-peak) at frequencies f = 11 kHz (for A and B) or 2 kHz (for C), with the lower electrodes connected to ground.

A miniature single wire probe operated at an overheat ratio of 1.8 on a constant-temperature anemometer is used to measure the streamwise velocity fluctuation u in the boundary layer, hence resolving the local wall shear stress τ_w for configurations A and B. Measurements are performed behind the actuator in spanwise and streamwise directions to capture the spanwise drag change and the streamwise drag recovery, respectively. Dantec time-resolved PIV system is used to capture the y-z plane behind the actuator pair with a view to study the size of streamwise vortices and their development in the turbulent boundary layer. The incoming flow is seeded with smoke generated from peanut oil by a TSI 9307-6 particles generator. The averaged seeding particle diameter is about 1 μm. A dual beam laser system (Litron LDY304-PIV, Nd: YLF), with a maximum energy output of 30 mJ/pulse, is used in conjunction with spherical and cylindrical lenses to form a light sheet of approximately 1.2 mm thick. Particle images are captured by a CCD camera (double frames, 2016 pixels × 2016 pixels). The sampling rate is 300 frames per second and the sampling duration is 1.33 s.

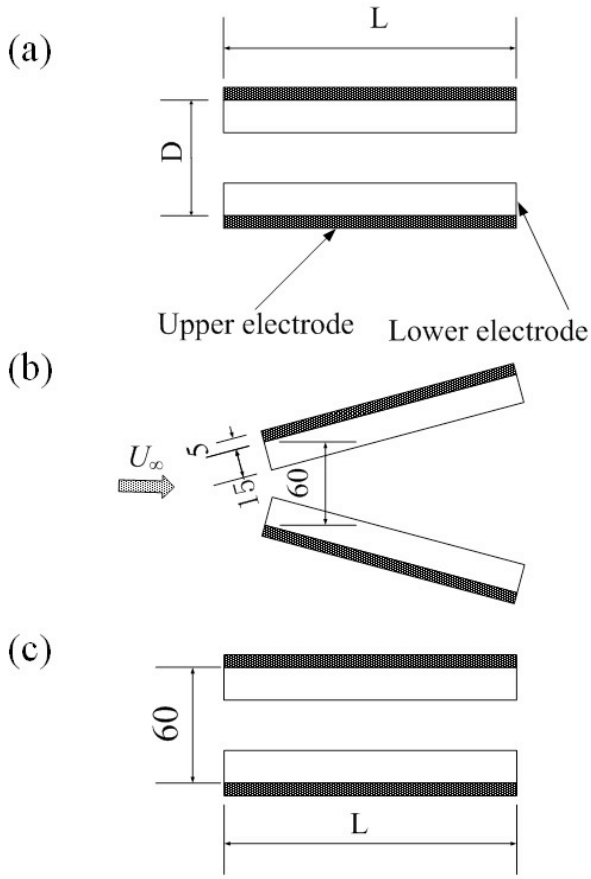

Figure 2. Schematics of the plasma actuator configurations: (a) configuration A; (b) configuration B; (c) configuration C.

For configuration C, a custom-built surface balance is deployed to measure the averaged skin-friction drag over an area covering 0.2 m × 0.1 m = 0.02 m^2 at x = 3.2 m (Fig. 3). The skin-friction drag on the flotation surface is resolved using the lever principle, thus allowing the conversion from the horizontal drag force to an amplified vertical force. The amplified force, pivoted about the knife-edge, is measured by a load-cell (Honeywell M34, range ±1kg) installed at 17 mm away from the knife-edge perpendicular to the horizontal axis. The amplified output signal

is acquired by the NI data acquisition card, with the sampling frequency and the sample time at 3000 Hz and 30 s, respectively. Details of the calibration method for the surface balance is given by Wong et al. 2015.

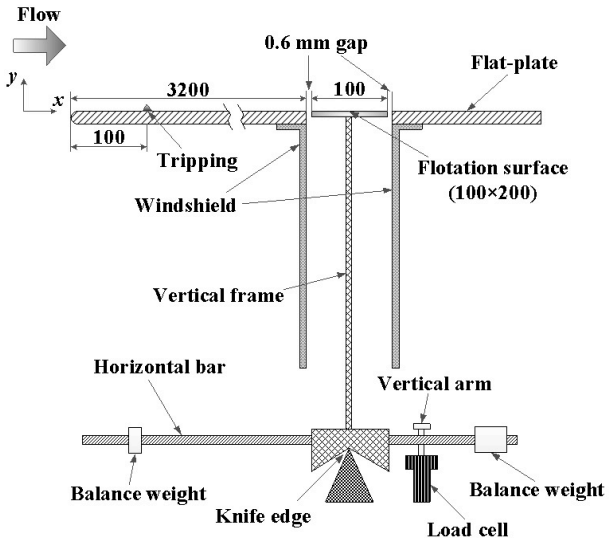

Figure 3. Schematic of experimental setup for skin friction measurement using surface balance.

RESULTS AND DISCUSSION

Effect of the size of plasma-generated vortices on drag reduction

At a constant V_a, the ionic wind velocity generated by the DBD plasma actuator in quiescent air would be approximately a constant irrespective to the change in L. In the presence of the turbulent boundary layer, the longer the actuator, the larger the vortex is produced since the plasma imparts the greater momentum into the flow. However, the increased L leads to the reduction of the maximum streamwise vorticity in the turbulent boundary layer.

In order to generate different vortex size while maintaining an approximately constant streamwise vorticity, different L (20, 40, 60, 80 and 100 mm) have been considered. Figure 4 shows the plasma-generated streamwise vortices in the y-z plane, captured at the trailing edge of a single plasma actuator. It can be seen that an approximately constant maximum streamwise vorticity of 200 s^{-1} is achieved in all actuators with different lengths due to fact that V_a is increased from 9 to 13 kV_{p-p}. In fact, a suitable V_a is searched for each actuator; the actuator with an L of 20, 60 and 100 mm correspond to 9, 11 and 13 kV_{p-p}, respectively. The lateral location of the vortex core increases with increasing electrode length due to the longer contact time with the DBD. Based on the PIV data achieved in Fig. 4, D is considered to be twice of the spanwise distance which covers both the primary and the secondary vortices generated by a single actuator. For examples, the D for an actuator pair with an L of 20, 60 and 100 correspond to 32, 60 and 80 mm, respectively.

Figure 5 shows the spanwise distribution of drag change Δc_f $(= (\bar{\tau}_w)_{off} - (\bar{\tau}_w)_{on} / (\bar{\tau}_w)_{off} \times 100\%)$ at 25 mm behind one pair of actuator, where $\bar{\tau}_w = \mu(\partial \overline{U}/\partial y)_{|y=0}$. The $(\bar{\tau}_w)_{on}$ and $(\bar{\tau}_w)_{off}$ are the wall shear stress in the viscous sublayer with and without plasma actuation, respectively. Note that the $\partial \overline{U}/\partial y$ near wall is estimated by linear fitting of five measurement points within the viscous sublayer. The spacing between two consecutive measurement points is 50 μm (0.33l) to warrant the accuracy of the Δc_f. The maximum local drag reduction is 21.9%, 26.7% and 37.9% for the actuator with L of 20, 60 and 100 mm, respectively. It is certain that large vortices generated by the long actuator (L = 100 mm) leads to higher local drag reduction compared to that with small vortices achieved by the short actuators, due to the large streamwise vorticity allows the removal of low momentum fluid near wall. However, there exists a large drag increase region when one considers the spanwise distribution of Δc_f behind an actuator. This is probably due to the fact that the actuator-generated vortices is strong in strength (200 s^{-1}). As a result, the relatively strong downwash enhances the drag increase. We believe that the long actuator, i.e. the large vortex size, should be used for the purpose of drag reduction due to the fact that a large drag reduction region exists between the vortex pair. More importantly, a relatively weak streamwise vorticity should be deployed in order to minimize the drag increase regions that exist on either sides of an actuator pair.

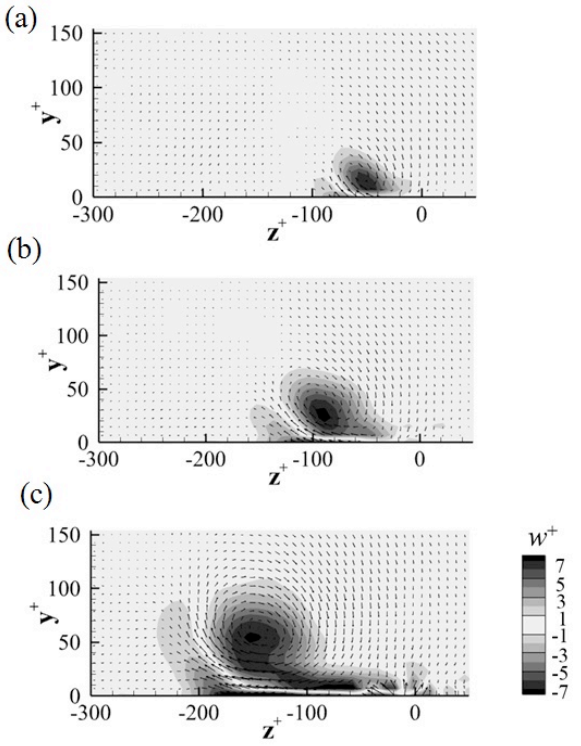

Figure 4. Plasma-actuator-generated vortices of different sizes (measured at the trailing edge of the actuator). (a) L = 20; (b) L = 60; (c) L = 100 mm (configuration A).

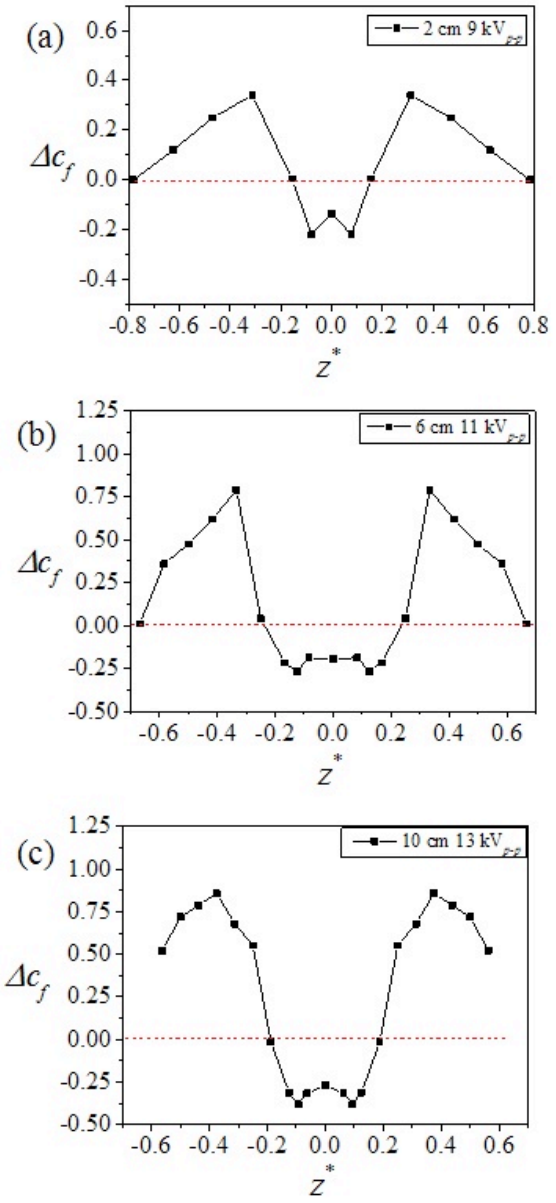

Figure 5. Spanwise distribution of Δc_f at 25 mm behind one pair of actuator; (a) L = 20 mm; (b) L = 60 mm; (c) L = 100 mm (configuration A).

Effect of the yawed plasma actuator on drag reduction

It can be seen in Fig. 6 that as β increases from 0 to 15°, the average Δc_f changes from positive to negative, indicating drag reduction. Evidently, the largest drag reduction is about 7.5% and is found at β = 15°. The drag reduction is deemed less at β > 15° and gradually becomes insignificant as β > 45°. Compared with the actuator at β = 0, the actuator at β = 15° generates weaker vortices, nevertheless, the size of vortices is somewhat similar to that at β = 0. Further increase of β larger than 15° would generate weaker and smaller vortices as compared to that at β = 0 (Juke & Choi 2012), thus leading to small drag reduction.

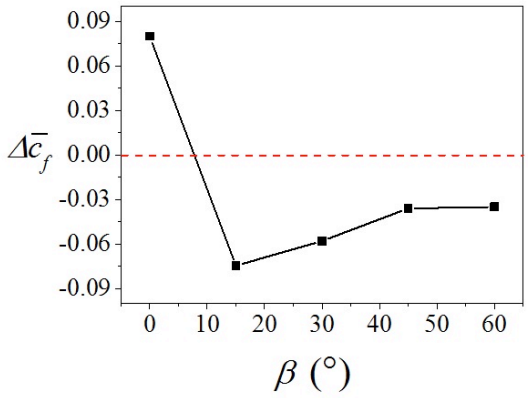

Figure 6. Dependence of the average Δc_f on the yaw angle (configuration B).

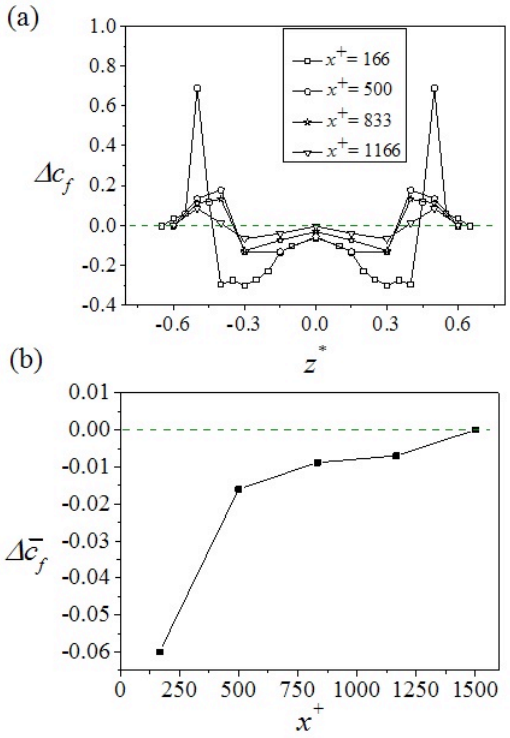

Figure 7. (a) Spanwise distributions of Δc_f behind one pair of actuators (configuration B); (b) Average Δc_f in the streamwise direction (configuration B).

It can be seen from Fig. 7a that the largest local drag reduction occurs at z^* = ±0.4 (z^* = z/D, z is the lateral distance measured from the midpoint between an actuator pair) and is about 29.5%. At 0.4 ⩾ z^* ⩾ 0.2 and -0.4 ⩽ z^* ⩽ -0.2, there exist drag reduction regions, which partially due to the upwash of the actuator-generated counter-rotating vortex pair that pumps the low-momentum fluid away from the wall. It should be noted that the spanwise distribution of Δc_f is appreciably different from Fig. 5a-c, though the largest local drag reduction is about the same. For instance, the drag due to the downwash of the actuator-

generated counter-rotating vortex pair is substantially reduced, probably due to the weak vortices generated by the yawed actuator. Through integrating the local Δc_f across $z^* = \pm 0.6$, the average Δc_f is estimated to be -6%, -1.6%, -0.9% and -0.7% at $x^+ = 166$, 500, 833 and 1166, respectively. It can be seen from Fig. 7b that the Δc_f changes rapidly at $166 \leqslant x^+ \leqslant 500$ and is close to the undisturbed value at $x^+ = 1500$. This observation is expected because the plasma-generated vortices would reduce in intensity and to mix themselves with the existing turbulent streamwise eddies with increasing x^+.

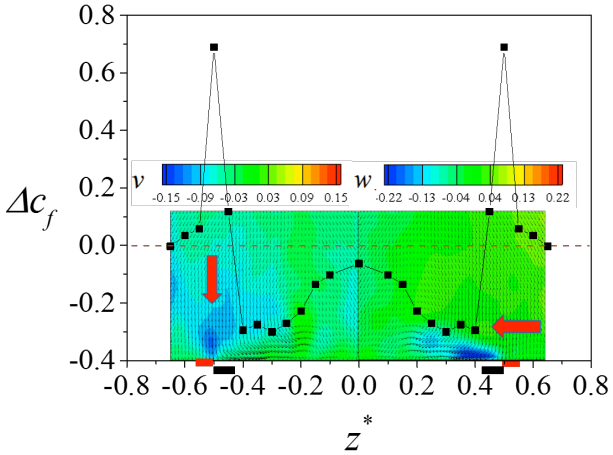

Figure 8. PIV-measured distribution of the normal v- and lateral w-component of velocity and the spanwise distribution of Δc_f behind the actuators at $x^+ = 166$ (configuration B).

Figure 8 presents the time-averaged PIV-measured distribution of the normal v- and lateral w-component of velocity and the spanwise distribution of Δc_f behind the actuators at $x^+ = 166$. The yawed actuator generates the w-component velocity due to the inclined body force. It can be seen from Fig. 8 that the large drag reduction in the immediate vicinity of the actuator ($0.4 \geqslant z^* \geqslant 0.3$ and $-0.4 \leqslant z^* \leqslant -0.3$) is associated closely to the spanwise wall jet which possibly interrupting the near wall vortex regeneration cycle by disrupting the naturally occurring distributions of streaks generated by previous or pre-existing streamwise vortices. Though different control method, we believe the mechanism of the suppressed vortex regeneration is somewhat similar to the one described in Schoppa & Hussain (1998). The spanwise wall jet becomes twisted into the streamwise direction by the oncoming freestream flow, thus leading to the formation of the vortex towards the center between the actuator pair. It is the upwash of the actuator-generated vortex pair, which pumps the low momentum fluid away from the wall, enhancing the drag reduction. In contrary, the drag increases at both edges of the upper electrodes as the result of the downwash of the vortex pair.

Effect of the length of the actuator on drag reduction

In general, drag reduction is achieved at $V_a \leqslant 4.5$ $kV_{p\text{-}p}$ for all actuators with different L, except $L = 100$ mm (Fig. 9). The maximum drag reduction are 9.0%, 17.7% and 25.0% for the actuator with $L = 150$ mm, 200 mm and 300 mm, respectively. Though PIV measurements were not performed, it is expected that at $x^+ = 166$ the vortex pair induced by the configuration C with $L = 100$ mm is relatively smaller, but stronger than those by the actuator with $L > 100$ mm. The very long actuator generates weaker and larger vortices that interact with the turbulent boundary layer, therefore causing drag reduction. At $L > 100$ mm, similar to Wong et al. 2015 which had $L = 200$ mm, their captured smoke-wire flow visualization of instantaneous flow structure in x-z plane at $y^+ = 24$ suggests that the low-speed streaks under control are stabilized, and hence interruption of vortex regeneration cycle and allowing substantial drag reduction. Figure 10 shows the dependence of Δc_f on the length of the actuator. Two observations can be made in Fig. 10. Firstly, at $L = 100$ mm, the actuator always produces drag increase irrespective to the V_a change. Secondly, at $L > 100$ mm, the drag reduction is greatly enhanced with increasing L, up to about 200 mm. At $L > 200$ mm, the drag reduction is less prominent, except for the actuator at $V_a = 4.5$ $kV_{p\text{-}p}$.

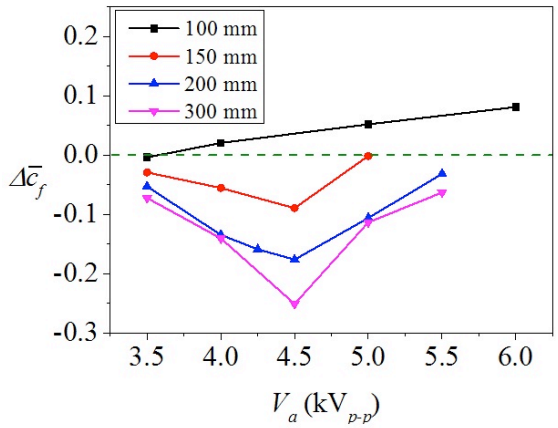

Figure 9. Dependence of the average Δc_f on the V_a (configuration C).

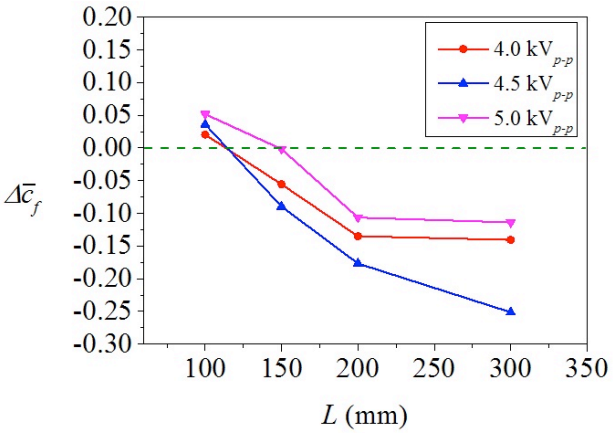

Figure 10. Dependence of the average Δc_f on the L (configuration C).

CONCLUSIONS

This work investigates the dependence of the size of the actuator-generated vortex, the yaw angle of the actuator, and the length of the actuator, on the drag change over a turbulent boundary layer. This work leads to following conclusions.

Large vortices generated by the long actuator (L = 100 mm) leads to the high local drag reduction compared to that with small vortices by the short actuators. We believe that the actuator-generated vortex should be large in size, but weak in strength, to generate effective drag reduction.

At β = 15°, the largest drag reduction is about 7%. It is found that large drag reduction in the immediate vicinity of the actuator is associated closely to the spanwise wall jet which possibly interrupting the near wall vortex regeneration cycle. Yet, the upwash of the actuator-generated vortex pair pumps low momentum fluid away from the wall, thus enhancing drag reduction.

The maximum drag reduction are 9.0%, 17.7% and 25.0% for the actuator with L = 150 mm, 200 mm and 300 mm, respectively. The very long actuator (L = 300 mm) generates weak and large vortices which interact with the turbulent boundary layer, therefore causing substantial drag reduction.

ACKNOWLEDGMENTS

C.W. Wong wishes to acknowledge support by the National Natural Science Foundation of China (NSFC) through grant 11502060 and from the Research Grants Council of the Shenzhen Government through grants JCYJ20160531193045101 and JCYJ20150513151706565.

REFERENCES

Choi, K. S., DeBisschop, J. R., and Clayton, B. R., 1998, "Turbulent Boundary-Layer Control by means of Spanwise-Wall Oscillation", *AIAA Journal*, Vol. 36, pp. 1157-1163.

Choi, K. S., and Clayton, B. R., 2001, "The Mechanism of Turbulent Drag Reduction with Wall Oscillation", *International Journal of Heat and Fluid Flow*, Vol. 22, pp. 1-9.

Choi, K. S., Jukes, T., and Whalley, R., 2011, "Turbulent Boundary-Layer Control with Plasma Actuators", *Philosophical Transactions of the Royal Society of London A: Mathematical, Physical and Engineering Sciences*, Vol. 369, pp. 1443-1458.

Corke, T. C., Enloe, C. L., and Wilkinson, S. P., 2010, "Dielectric Barrier Discharge Plasma Actuators for Flow Control", *Annual Review of Fluid Mechanic*, Vol. 42, pp. 505–530.

Jukes, T. N., and Choi, K. S. 2012, "Dielectric-Barrier-Discharge Vortex Generators: Characterisation and Optimisation for Flow Separation Control", *Experiments in Fluids*, Vol. 52(2), pp. 329-345.

Moreau, E., 2007, "Airflow Control by Non-Thermal Plasma Actuators", *Journal of Physics D: Applied Physics*, Vol. 40, pp. 605–636.

Schoppa, W., and Hussain, F., 1998, "A Large-Scale Control Strategy for Drag Reduction in Turbulent Boundary Layers", *Physics of Fluids*, Vol. 10, pp. 1049-1051.

Whalley, R. D., and Choi, K. S., 2014, "Turbulent Boundary-Layer Control with Plasma Spanwise Travelling Waves", *Experiments in Fluids*, Vol. 55, pp. 1-16.

Wong, C.W., Zhou, Y., Li, Y.Z., and Li, Y.P., 2015, "Active Drag Reduction in a Turbulent Boundary Layer based on Plasma-Actuator-Generated Streamwise Vortices", *Proceedings of the Turbulence and Shear Flow Phenomena (TSFP9)*, The University of Melbourne, Australia, Paper 209.